Existence domain of electrostatic solitary waves in the lunar wake

R. Rubia,[a] S. V. Singh,[b] and G. S. Lakhina[c]
Indian Institute of Geomagnetism, Navi Mumbai, India

(Received 28 November 2017; accepted 9 February 2018; published online 1 March 2018)

Electrostatic solitary waves (ESWs) and double layers are explored in a four-component plasma consisting of hot protons, hot heavier ions (He^{++}), electron beam, and suprathermal electrons having κ-distribution using the Sagdeev pseudopotential method. Three modes exist: slow and fast ion-acoustic modes and electron-acoustic mode. The occurrence of ESWs and their existence domain as a function of various plasma parameters, such as the number densities of ions and electron beam, the spectral index, κ, the electron beam velocity, the temperatures of ions, and electron beam, are analyzed. It is observed that both the slow and fast ion-acoustic modes support both positive and negative potential solitons as well as their coexistence. Further, they support a "forbidden gap," the region in which the soliton ceases to propagate. In addition, slow ion-acoustic solitons support the existence of both positive and negative potential double layers. The electron-acoustic mode is only found to support negative potential solitons for parameters relevant to the lunar wake plasma. Fast Fourier transform of a soliton electric field produces a broadband frequency spectrum. It is suggested that all three soliton types taken together can provide a good explanation for the observed electrostatic waves in the lunar wake. *Published by AIP Publishing.*
https://doi.org/10.1063/1.5017638

I. INTRODUCTION

Satellite observations have substantiated the existence of electrostatic solitary waves (ESWs) in several regions of the Earth's magnetosphere, viz., auroral region,[1,2] magnetotail,[3] plasma sheet boundary layer (PSBL),[4] magnetopause,[5] bow shock,[6] Van Allen radiation belt,[7,8] as well as in the solar wind[9,10] and lunar wake.[11] Recently, Vasko *et al.*[8] have provided the first direct identification of the ESWs observed by Van Allen probe in terms of electron-acoustic solitons and double layers (DL). ESWs are found to have bipolar or tripolar signatures in the electric field component parallel to the background magnetic field. They are generally associated with ion or/and electron beams.

The interaction of the solar wind with the moon results in a void in the "night-side" due to the absorbance of the solar wind plasma by the lunar surface. This void is referred to as the lunar wake. The absence of intrinsic magnetic field and sufficiently low conductivity of the moon facilitates the easy penetration of the solar wind magnetic field through the moon. The density gradient between the lunar wake and the solar wind drives the solar wind plasma to refill the lunar wake along the magnetic field lines through ambipolar diffusion.[12–15] On the basis of the observations of SELENE (KAGUYA) spacecraft, Hashimoto *et al.*[11] reported the observations of ESWs near the Moon in the solar wind and in the lunar wake. Tao *et al.*[14] provided a detailed analysis of the electrostatic waves observed in the lunar wake during the first flyby of the ARTEMIS mission.

The satellite observations of the ESWs have resulted in a surge in the theoretical studies on ESWs in multi-species unmagnetized and magnetized plasmas.[15–52] Watanabe and Taniuti[18] reported the existence of electron-acoustic solitons in a two-electron-temperature plasma. Gary and Tokar[23] showed the propagation of electron-acoustic mode with frequencies between the ion and electron plasma frequencies in a three-component plasma consisting of ions, hot electrons, and cool electrons. Verheest *et al.*[28] and Cattaert *et al.*[29] showed that two-electron-temperature plasma can support the existence of both positive and negative potential electron-acoustic solitons when the inertia of hot electron is retained. Lakhina *et al.*[31] investigated the properties of ion- and electron-acoustic solitons in an unmagnetized three-component plasma comprising of cold and hot electrons and ions. This model was extended by Lakhina *et al.*[32] to include a hot ion beam. They found that three modes, viz., slow and fast ion-acoustic mode and electron-acoustic mode exist. The slow and fast ion-acoustic mode was found to support only positive potential solitons, while electron-acoustic mode supported both positive and negative potential solitons. Nsengiyumva *et al.*[48] reported the existence of stopbands for fast ion-acoustic solitons in a three-component plasma with cold and warm ions and Boltzmann electrons.

Lakhina and Singh[53] and Rubia *et al.*[54] proposed a generation mechanism for the observed weak double layers (WDLs) and low-frequency coherent electrostatic waves in the solar wind at 1 AU by WIND spacecraft in terms of slow and fast ion-acoustic solitons and double layers. The solar wind plasma was modelled as a three-component plasma consisting of hot protons, hot helium ions, and electrons having a kappa distribution.

There are two main mechanisms for the generation of ESWs observed in space plasmas. The most popular mechanism is based on the BGK (Bernstein-Green-Kruskal) modes or phase space holes[55–58] where the trapped particle population

[a]Electronic mail: rubi.r92@gmail.com
[b]Electronic mail: satyavir@iigs.iigm.res.in
[c]Electronic mail: gslakhina@gmail.com

is essential. Various kinetic simulations have shown that nonlinear saturation of electron beam instabilities lead to the formation of isolated potential structures, equivalent to the BGK modes or phase space holes, which can successfully reproduce the electrostatic solitary waveforms.[3,4,59–62] However, the phase space holes observed in these simulations are not stable; they are likely to either merge or breakup during the evolution of the instability. The second mechanism for ESWs is based on either ion- or electron-acoustic solitons and double layers described by the fluid models. The effects of trapped particle populations are neglected in fluid models. The fluid approach is justified for scale lengths greater than the Debye length. Therefore, the fluid models cannot accurately describe the properties of ESWs having widths of the order of Debye length or less. In this paper, the ESWs are described in terms of ion- and electron-acoustic solitons and double layers given by the fluid models.

A theoretical model to explain the occurrence of electrostatic waves observed in the lunar wake during the first flyby of ARTEMIS mission[14] was proposed by Rubia *et al.*[15] in terms of slow and fast ion-acoustic solitons and electron-acoustic solitons. They were able to explain the main observed characteristics of the waves. They used a four-component model comprising of hot protons, hot heavier ions (He^{++}), electron beam, and suprathermal electrons having κ-distribution. In this paper, we extend their work to study the occurrence and the existence domain of the slow and fast ion-acoustic solitons and electron-acoustic solitons existing in the lunar wake. We emphasize that our model deals with the time stationary state of the plasma system when the plasma instabilities, if excited initially by the electron beam, have been saturated.

The paper is organized as follows. In Sec. II, the theoretical model for the lunar wake plasma is presented. For a detailed theory of the lunar wake model, kindly refer to the paper of Rubia *et al.*[15] For ease of reference, we provide the final expression for Sagdeev pseudopotential and the dispersion relation. The numerical results are given in Sec. III and the results are summarized in Sec. IV.

II. THEORETICAL MODEL

A homogeneous, collisionless, and magnetized four-component plasma comprising of protons (N_{p0}, T_p), heavier ions, i.e., alpha particles, He^{++} (N_{i0}, T_i), electron beam (N_{b0}, T_b, V_{b0}), and suprathermal electrons following κ-distribution (N_{e0}, T_e) has been used for modelling the lunar wake plasma.[15] Here, the inertia of the hot electrons following κ-distribution has been neglected. The ESWs are assumed to be propagating parallel to the ambient magnetic field, $\vec{B}_0$. The dynamics of the nonlinear waves can be described by the energy equation[15]

$$\frac{1}{2}\left(\frac{d\phi}{d\xi}\right)^2 + S(\phi, M) = 0. \tag{1}$$

Here, ϕ is the electrostatic potential and ξ is the transformation coordinate given by $\xi = x - Mt$, where $M = V/C_a\left(C_a = \sqrt{T_e/m_p}\right)$ is the Mach number. The Sagdeev potential, $S(\phi, M)$, is given below

$$\begin{aligned}
S(\phi,M) = {} & \frac{n_{p0}}{6\sqrt{3\sigma_p}}\left\{\left(M+\sqrt{3\sigma_p}\right)^3 - \left[\left(M+\sqrt{3\sigma_P}\right)^2 - 2\phi\right]^{3/2} - \left(M-\sqrt{3\sigma_p}\right)^3 + \left[\left(M-\sqrt{3\sigma_p}\right)^2 - 2\phi\right]^{3/2}\right\} \\
& + \frac{n_{i0}}{6\sqrt{3\sigma_i}}\left\{\left(\frac{M}{\sqrt{\mu_{pi}}}+\sqrt{3\sigma_i}\right)^3 - \left[\left(\frac{M}{\sqrt{\mu_{pi}}}+\sqrt{3\sigma_i}\right)^2 - 2Z_i\phi\right]^{3/2} - \left(\frac{M}{\sqrt{\mu_{pi}}}-\sqrt{3\sigma_i}\right)^3\right. \\
& \left. + \left[\left(\frac{M}{\sqrt{\mu_{pi}}}-\sqrt{3\sigma_i}\right)^2 - 2Z_i\phi\right]^{3/2}\right\} + \frac{n_{b0}}{6\sqrt{3\sigma_b}}\left\{\left(\frac{M-V_{b0}}{\sqrt{\mu_{pe}}}+\sqrt{3\sigma_b}\right)^3 - \left[\left(\frac{M-V_{b0}}{\sqrt{\mu_{pe}}}+\sqrt{3\sigma_b}\right)^2 + 2\phi\right]^{3/2}\right. \\
& \left. + \left[\left(\frac{M-V_{b0}}{\sqrt{\mu_{pe}}}-\sqrt{3\sigma_b}\right)^2 + 2\phi\right]^{3/2} - \left(\frac{M-V_{b0}}{\sqrt{\mu_{pe}}}-\sqrt{3\sigma_b}\right)^3\right\} + n_{e0}\left[1 - \left(1 - \frac{\phi}{\kappa - 3/2}\right)^{-\kappa+3/2}\right].
\end{aligned} \tag{2}$$

Equation (2) has been written in the symbolic form where the operation of a square root on a squared expression returns the same expression, e.g., $\sqrt{(M\pm\sigma_j)^2} = M\pm\sigma_j$. n_{p0}, n_{i0}, n_{b0}, n_{e0} correspond to the normalized number density of protons, ions, electron beam, and suprathermal electrons, respectively. $\mu_{pj} = m_p/m_j$, where m_j is the mass of the jth species, where j = p, i, b, and e for protons, heavier ions, electron beam, and suprathermal electrons, respectively. $\sigma_j = T_j/T_e$, where, T_j is the temperature of the jth species. $Z_j = +1(-1)$ for protons (electrons), and $Z_j = +2$ for heavier ions. V_{b0} is the electron beam drift velocity along the ambient magnetic field, $\vec{B}_0$.

For soliton solutions to exist, the Sagdeev pseudopotential $S(\phi, M)$ must satisfy the following conditions: (i) $S(\phi, M) = 0$, $dS(\phi, M)/d\phi = 0$, and $d^2S(\phi, M)/d\phi^2 < 0$ at $\phi = 0$, (ii) $S(\phi, M) = 0$ at $\phi = \phi_{max}$ (ϕ_{max} is the maximum amplitude), and (iii) $S(\phi, M) < 0$ for $0 < |\phi| < |\phi_{max}|$.

Further, in addition to the soliton conditions (i)–(iii), for a double layer solution, (iv) $dS(\phi,M)/d\phi = 0$ at $\phi = \phi_{max}$ has to be satisfied. The critical Mach number, M_0, above which $M > M_0$, the soliton solution exists is governed by the following expression for the dispersion relation[15]

$$\frac{n_{p0}}{M^2 - 3\sigma_p} + \frac{n_{i0}Z_i^2}{\frac{M^2}{\mu_{pi}} - 3\sigma_i} + \frac{n_{b0}}{\frac{(M - V_{b0})^2}{\mu_{pe}} - 3\sigma_b} = n_{e0}\left(\frac{2\kappa - 1}{2\kappa - 3}\right). \tag{3}$$

The numerical solution of Eq. (3) gives three physical real positive roots for the lunar wake plasma parameters. The smallest and intermediate roots are slow and fast ion-acoustic modes, respectively, and the largest root is the electron-acoustic mode.[32] The fast ion-acoustic mode is similar to the usual ion-acoustic mode of the proton-electron plasma. The slow ion-acoustic mode is a new ion-acoustic mode modified due to the presence of heavier ions. It is an ion-ion hybrid mode that requires essentially two ion species having different thermal velocities or a relative streaming between the ions.[53]

III. NUMERICAL RESULTS

In this section, the numerical results for slow and fast ion-acoustic and electron-acoustic modes obtained by solving Eqs. (2) and (3) are presented for lunar wake plasma parameters.[9,14,15,53] The results for each mode, i.e., slow, fast, and electron-acoustic are as follows:

A. Slow ion-acoustic solitons

Figure 1 shows the existence curve for the slow ion-acoustic solitons as a function of the electron beam velocity, V_{b0} for the parameters relevant to the lunar wake plasma.[14,15] The normalized parameters considered here are $n_{i0} = 0.05$, $n_{b0} = 0.01$, $\sigma_p = 0.2$, $\sigma_i = 0.4$, $\sigma_b = 0.0025$, and $\kappa = 6$. Panel (a) corresponds to the variation of $M_{max} - M_0$ with V_{b0}. M_{max} is the maximum Mach number beyond which the soliton solution ceases to exist. The electric potential amplitude ϕ corresponding to M_{max} is considered as ϕ_{max}. For $0 \le V_{b0} < 4.3$ (region-I), we have positive potential solitons. In region-II, $4.3 \le V_{b0} < 4.7$, and IV, $5.1 \le V_{b0} < 5.2$, we observe negative potential solitons. Region-III is a "forbidden gap" region for $4.7 \le V_{b0} < 5.1$. "Forbidden gap" is the region in which the solitons cannot propagate.[26,49] The occurrence of the "forbidden gap" can be attributed to the fact that the root of Eq. (3) corresponding to the slow ion-acoustic mode becomes complex. Region-V (between the red-dashed lines), $5.2 \le V_{b0} \le 5.6$, corresponds to the region of coexistence of both positive and negative polarity solitons. The variation of corresponding maximum electrostatic potential, ϕ_{max} with V_{b0}, is shown in panel (b). In region-V, the violet + sign and the blue circles on ϕ_{max} show the existence of positive and negative potential solitons, respectively. For further increase in V_{b0}, positive potential soliton occurs as shown in region-VI. Here, the upper limit M_{max} on the Mach number for the positive potential slow ion-acoustic solitons is provided by the restriction that the number density of heavier ions, n_i, be real. This is consistent with the results of Rubia *et al.*[15,54] In the case of negative potential slow ion-acoustic soliton, the restriction is provided by the requirement that the number density of electron beam, n_b, be real.

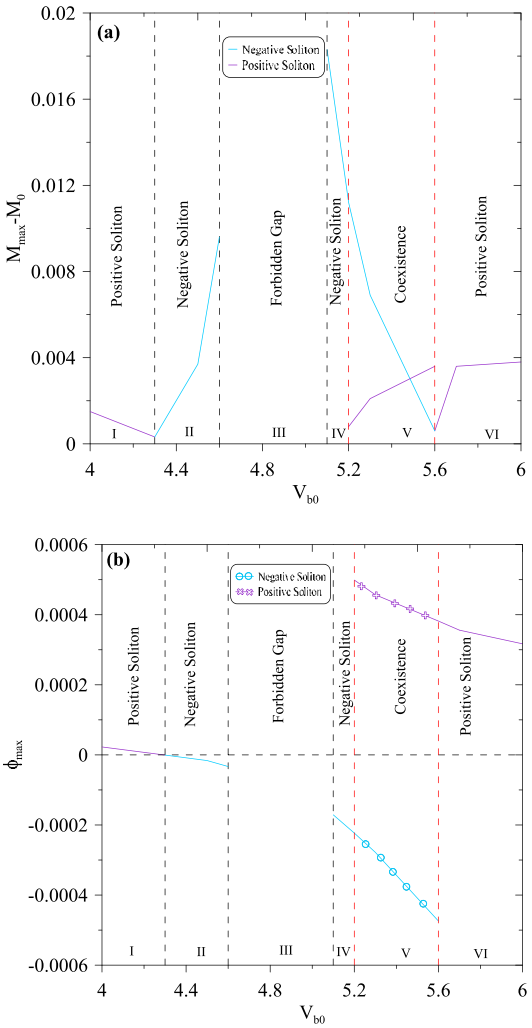

FIG. 1. Existence domain of slow ion-acoustic soliton as a function of V_{b0} for the normalized parameters: $n_{i0} = 0.05$, $n_{b0} = 0.01$, $\sigma_p = 0.2$, $\sigma_i = 0.4$, $\sigma_b = 0.0025$, and $\kappa = 6$. Panel (a): $M_{max} - M_0$, Panel (b): ϕ_{max}. Positive solitons (regions-I and VI), negative solitons (regions-II and IV), "forbidden gap" (region-III), and coexistence (region-V) of both positive and negative potential solitons. In region-V, the violet + signs and blue circles on ϕ_{max} show the positive and negative potential solitons, respectively.

We observe from Fig. 1 that both $M_{max} - M_0$ and ϕ_{max} decrease with V_{b0} in region-I. This signifies that the region in which soliton exists decreases as the electron beam velocity, V_{b0}, increases. In region-II, $M_{max} - M_0$ increases whereas it decreases in region-IV. In the region-V corresponding to the coexistence of both positive and negative polarity solitons, $M_{max} - M_0$ decreases for negative potential solitons while it increases for positive potential solitons. The maximum amplitude, ϕ_{max}, becomes negative and decreases in regions-II and IV. ϕ_{max} corresponding to the negative potential soliton in the region of coexistence (region-V) also decreases with increase in V_{b0}. Similarly, ϕ_{max} for the positive potential soliton decreases in both regions V and VI.

Figures 2(a) and 2(b) show the variation of critical (M_0) and maximum (M_{max}) Mach numbers and maximum value of the electrostatic potential, ϕ_{max}, with κ and n_{i0}, respectively, for the slow ion-acoustic mode for the plasma parameters: $n_{i0} = 0.05$, $n_{b0} = 0.01$, $\sigma_p = 0.2$, $\sigma_i = 0.4$, $\sigma_b = 0.0025$, $V_{b0} = 4$, and $\kappa = 6$. Here, for a particular variation, apart from the parameter being varied, the rest of the parameters remains the same.

From 2(a), we observe that both M_0 and M_{max} gradually increase from $\kappa = 2$ and remains almost constant after $\kappa = 4$. ϕ_{max} is found to increase gradually with the increase in κ. From 2 (b), we observe that M_0 increases with increase in n_{i0}. M_{max} increases gradually with n_{i0} till $n_{i0} = 0.49$. ϕ_{max} increases gradually with n_{i0} till $n_{i0} = 0.4$. For further increase in n_{i0}, ϕ_{max} decreases till $n_{i0} = 0.49$. At $n_{i0} = 0.5$, both M_{max} and ϕ_{max} show a sudden increase. Further, we found that at $n_{i0} = 0.5$, i.e., when the proton number density, $n_{p0} = 0$, the upper limit on the Mach number, M_{max}, for slow ion-acoustic solitons exceeds the critical Mach number $M_0 = 0.7746$ for fast ion-acoustic solitons. The M_{max} and ϕ_{max} for both slow and fast ion-acoustic soliton coincide at $n_{i0} = 0.5$. This essentially signifies that at $n_{i0} = 0.5$, we only have one ion-acoustic soliton. The existence domain for the solitons, i.e., $M_{max} - M_0$, increases with n_{i0}.

The existence domain for the slow ion-acoustic solitons as a function of n_{b0} for the normalized parameters corresponding to Fig. 2 was explored (not shown). We found that M_0, M_{max}, and ϕ_{max} show a similar trend, i.e., initially gradually decreases and then remains almost constant. This signifies that the number density of beam electrons does not significantly affect the existence of the slow ion-acoustic solitons.

Figure 3 depicts the existence domain for the slow ion-acoustic solitons/double layers (DL) as a function of σ_i for the normalized parameters corresponding to Fig. 2. The existence domains corresponding to positive and negative potential solitons and double layers are clearly demarcated with vertical dashed lines. The variation of $M_{max} - M_0$ with σ_i is shown in Panel (a). We found that no soliton solution exists for $0 \le \sigma_i < 0.02$ as the root of Eq. (3) corresponding to slow ion-acoustic mode becomes complex. In region-I,

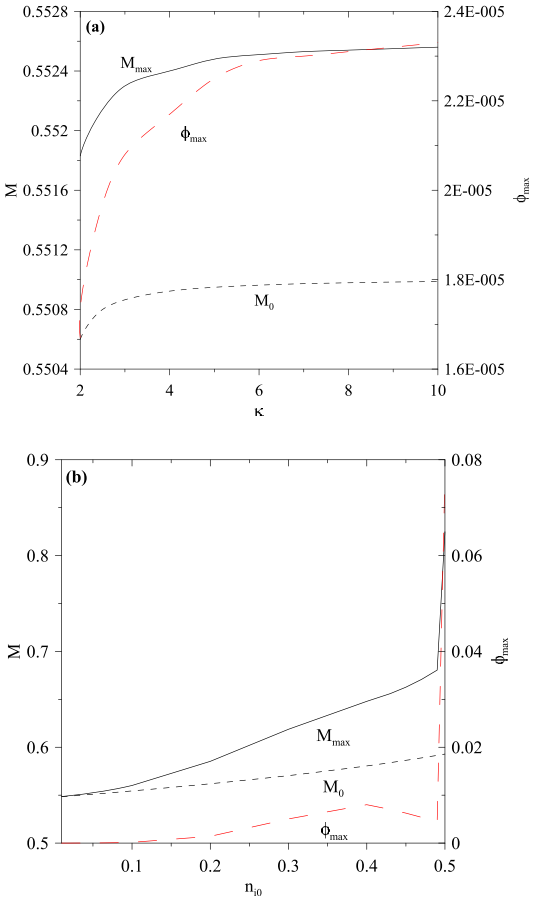

FIG. 2. Slow ion-acoustic solitons: Variation of critical Mach number, M_0(dashed curves), maximum Mach number, M_{max} (solid curves), and maximum value of the potential, ϕ_{max} (long-dashed red curve) with (a) κ and (b) n_{i0} for the normalized parameters: $n_{i0} = 0.05$, $n_{b0} = 0.01$, $\sigma_p = 0.2$, $\sigma_i = 0.4$, $\sigma_b = 0.0025$, $V_{b0} = 4$, and $\kappa = 6$. For a particular variation, apart from the parameter being varied, the rest of the parameters remains the same. Here the Y-axis on the left hand side (LHS) shows the scale for Mach number, while on the right hand side (RHS) shows the scale for maximum electric potential amplitude ϕ_{max}.

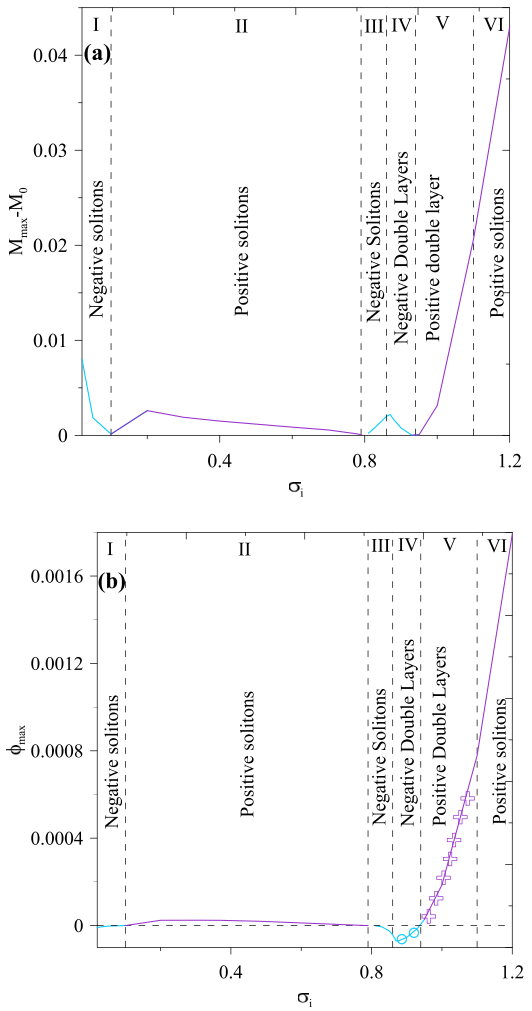

FIG. 3. Existence domain of slow ion-acoustic solitons (a) $M_{max} - M_0$ (b) maximum amplitude, ϕ_{max}, as a function of σ_i for the parameters of Fig. 2. Positive solitons (regions-II and VI) and negative solitons (regions-I and III). At $\sigma_i = 0.8$, slow ion-acoustic solitons ceases to exist. Double layers: negative (region-IV) and positive (region V). The circles and + signs on ϕ_{max} show the existence of negative and positive double layers, respectively.

$0.02 \leq \sigma_i < 0.2$, and region-III, $0.8 < \sigma_i < 0.87$, we have negative potential solitons. In region-I, the maximum attainable amplitude, M_{max}, of the negative potential soliton is limited by the requirement that the number density of electron beam, n_b, be real, while for the negative potential soliton in region-III, the limitation is provided by the violation of the conditions to be satisfied by the Sagdeev pseudopotential for the soliton solution to exist.[54] Here, the requirement that $S(\phi, M) = 0$ at $\phi = \phi_{max}$ and $S(\phi, M) < 0$ for $0 < |\phi| < |\phi_{max}|$ is violated. In region-II ($0.2 \leq \sigma_i < 0.8$) and region-VI ($1.1 < \sigma_i \leq 1.2$), we have positive potential solitons. At $\sigma_i = 0.8$ ($T_i = 4T_p$), the slow ion-acoustic mode ceases to exist and there is a gap in the existence domain region around $\sigma_i = 0.8$. This is consistent with the results of Lakhina and Singh[53] and Rubia *et al.*[54] In region-IV ($0.87 \leq \sigma_i < 0.94$), we have negative double layers; this is followed by a positive double layer in region-V ($0.94 \leq \sigma_i \leq 1.1$). The variation of corresponding maximum electrostatic potential, ϕ_{max}, with σ_i is depicted in panel (b). The empty circles (region-IV) and the + signs (region-V) on the ϕ_{max} curve show the existence of negative and positive double layers, respectively.

We observe that $M_{max} - M_0$ decreases, while ϕ_{max} increases in region-I. In region-II, both $M_{max} - M_0$ and ϕ_{max} initially increase and then decrease till $\sigma_i < 0.8$. The $M_{max} - M_0$ curve increases in region-III followed by a decrease in region-IV. ϕ_{max} decreases in region-III followed by an increase in region-IV. This is followed by an increase in both the $M_{max} - M_0$ and ϕ_{max} in region-V and VI. The trend shown by the existence domain as a function of σ_i is similar to the reported trend of the slow ion-acoustic solitons by Rubia *et al.*[54]

The profiles of normalized potential ϕ with ξ for the slow ion-acoustic solitons are depicted in Fig. 4 for the normalized parameters: $n_{i0} = 0.05$, $n_{b0} = 0.01$, $\sigma_p = 0.2$, $\sigma_b = 0.0025$, $V_{b0} = 4$, and $\kappa = 6$. For $\sigma_i = 0.88$, the slow ion-acoustic mode supports negative potential double layers as shown in Fig. 4(a). Here, the soliton amplitude increases, while the width decreases with increase in the Mach number until M_{max} is reached. Here, the upper limit on the Mach number is provided by the occurrence of a negative double layer at $M = 0.8109639$. For $\sigma_i = 1.0$, the slow ion-acoustic mode supports positive potential double layers as shown in Fig. 4(b). Here, the soliton amplitude as well as the width increases with increase in the Mach number until M_{max} is reached. Here, the upper limit on the Mach number is provided by the occurrence of a positive double layer at $M = 0.8508238833$. A similar trend of increase in the width with increasing amplitude in the auroral region was reported by Dombeck *et al.*[63] on the basis of POLAR satellite observations. Ghosh and Lakhina[64] referred to the behavior as "anomalous," as in K-dV (small amplitude) solitons; generally, the width is found to decrease with increase in amplitude. However, here the width increases with the amplitude. For clarity, the double layer profile is marked as DL in the figure.

The existence domain for the slow ion-acoustic solitons as a function of σ_b for the parameters of Fig. 2 was explored (not shown to conserve space). We found that no soliton solution exists for $0 < \sigma_b < 0.002$ as the root of Eq. (3) for the slow ion-acoustic mode becomes complex in this region. Negative potential soliton occurs at a singular point corresponding to $\sigma_b = 0.002$. With a further increase in σ_b ($\sigma_b > 0.002$), we have positive potential solitons. Initially, both $(M_{max} - M_0)$ and ϕ_{max} were found to increase gradually with σ_b, followed by a slight decrease with a further increase in σ_b.

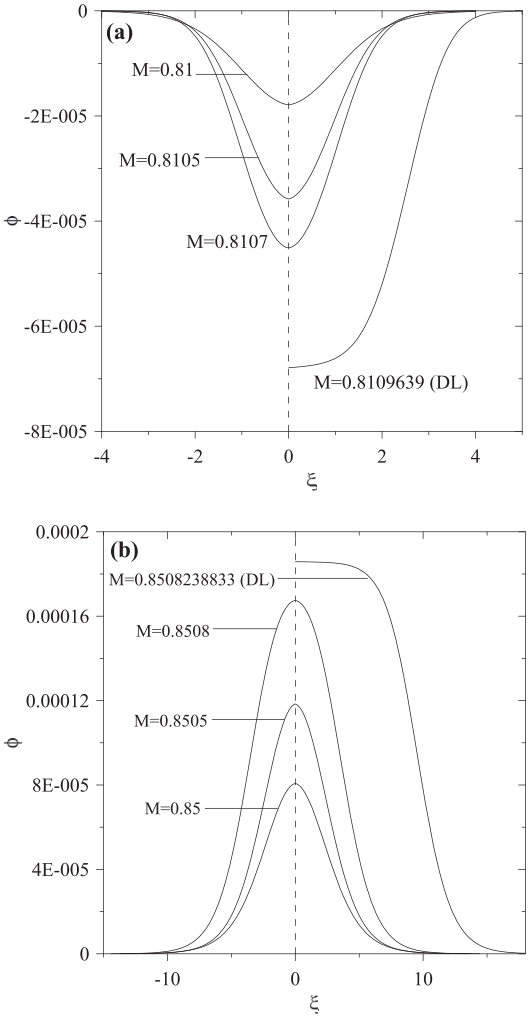

FIG. 4. The negative [panel (a)] and positive [panel (b)] potential slow ion-acoustic double layers for Fig. 2 parameters. Here, $\sigma_i = 0.88$ for negative double layer and $\sigma_i = 1.0$ for positive double layer.

B. Fast ion-acoustic solitons

Figure 5 shows the existence domain for fast ion-acoustic solitons varying with the electron beam velocity, V_{b0}, for the lunar wake plasma parameters (refer Fig. 1). Panel (a) shows the variation of $M_{max} - M_0$ with V_{b0}, while panel (b) shows the variation of corresponding maximum electric potential amplitude, ϕ_{max} with V_{b0}. For $0 \leq V_{b0} < 4.5$ (region-I), we have positive potential solitons. In region-II, $4.5 \leq v_{b0} < 5.1$, and region-V, $8.5 < V_{b0} < 10$, we have negative potential solitons. This is followed by a "forbidden gap," $5.1 \leq V_{b0} < 7.8$ (region-III). The occurrence of "forbidden-gap" can be attributed to that the

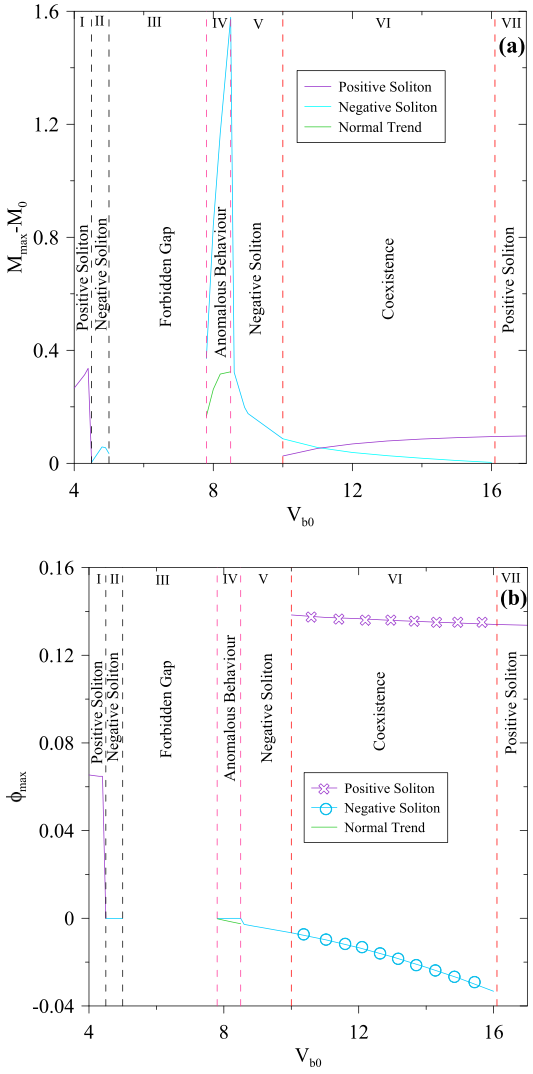

FIG. 5. Fast ion-acoustic solitons: Existence domains as a function of V_{b0} for the parameters of Fig. 1. Positive solitons (regions-I and VII), negative solitons (regions-II and V), "forbidden gap" (region-III), and "anomalous behaviour" is observed in region-IV. The green curve depicts the normal trend of the solitons. In region-V, coexistence of both positive and negative potential solitons occurs. In this region, the violet + signs and the blue circles on ϕ_{max} show the positive and negative potential solitons, respectively.

solution of Eq. (3) gives complex root corresponding to the fast ion-acoustic mode. In region-IV, $7.8 \leq V_{b0} \leq 8.5$, we observe an "anomalous behaviour" of the solitons. The green line in both $M_{max} - M_0$ and ϕ_{max} curve shows the "normal trend." In this region, initially the amplitude of the fast ion-acoustic soliton increases with the increase in the Mach number till some Mach number, M_{max1}. This trend of increase in amplitude with the Mach number is referred to as the "normal trend" and is observed for all solitons. Immediately after M_{max1} for further increase in the Mach number, we have an "anomalous behavior," i.e., decrease in the amplitude with the increase in the Mach number. Further, we observe crossing of two potential curves for different Mach numbers, which is not expected. None of the densities becomes complex in the case of "anomalous behaviour" as well as none of the stipulated soliton conditions are violated. There is no gap between the "normal trend" and "anomalous behavior." The reason for the existence of such an "anomalous behaviour" is not known, and it is being investigated and will be reported elsewhere.

In region-VI (between the red-dashed lines), $10 \leq V_{b0} \leq 16.1$, we have coexistence of both positive and negative potential solitons. The violet + signs and the blue circles on ϕ_{max} show the existence of positive and negative potential solitons, respectively; a further increase in V_{b0} gives positive potential solitons (region-VII). The limitation on the maximum attainable Mach number, M_{max}, for a positive potential soliton is attributed to the requirement that the number density of protons, n_p, should remain real. While for the negative potential solitons, the limitation is provided by the requirement that the number density of electron beam, n_b, should remain real. This is consistent with the results of Rubia *et al.*[15,54]

We observe that the $M_{max} - M_0$ increases gradually in region-I. In the region of "anomalous behaviour," the increase is drastic followed by a decrease in region-V. In the region-VI corresponding to coexistence, $M_{max} - M_0$ decreases for the negative potential solitons, while it increases for the positive potential solitons which persists in region-VII corresponding to positive solitons. The crossover of the negative and positive potential in region-VI indicates that initially the existence domain for the positive potential solitons is less than that of the negative potential solitons till $\sim V_{b0} = 11$. After that, the existence domain for positive soliton is more than that of the negative soliton. ϕ_{max} shows a decrease in region-I. In region-II and IV corresponding to the "anomalous behavior," the curve remains almost constant. ϕ_{max} for negative solitons in both regions-V and VI decreases with the increase in V_{b0}. ϕ_{max} decreases with the increase in V_{b0} for positive solitons in both regions-VI and VII.

The existence domain (not shown to conserve space) for the fast ion-acoustic solitons as a function of κ, n_{i0}, σ_i, n_{b0}, and σ_b was explored for the parameters of Fig. 2. The behaviors of $(M_{max} - M_0)$ and ϕ_{max} against variation of the parameters κ, n_{b0}, and σ_b were found to be similar to that of slow ion-acoustic solitons, except that the magnitudes of ϕ_{max} were always greater than the slow ion-acoustic solitons case. The $(M_{max} - M_0)$ was found to decrease with the increase in n_{i0} till $n_{i0} = 0.49$. Both M_0 and M_{max} were found to almost remain constant with the increase in σ_i. However, ϕ_{max} increases with σ_i.

C. Electron-acoustic solitons

Electron-acoustic mode is found to support only negative potential solitons for the lunar wake plasma parameters. This is expected as we know that the existence of positive potential electron-acoustic soliton requires the inertia of the hot electron to be included.[28,40] The variation of critical Mach number, M_0, maximum Mach number, M_{max}, and maximum value of electrostatic potential, ϕ_{max}, with V_{b0}, κ, n_{b0}, and σ_b for the normalized parameters corresponding to Fig. 2, is depicted in Figs. 6(a)–6(d), respectively, for the electron-acoustic mode. Here, for a particular variation, apart from the parameter being varied, the rest of the parameters remains the same.

From Fig. 6(a), we observe that both M_0 and M_{max} increase linearly with V_{b0}, while the existence domain, i.e.,

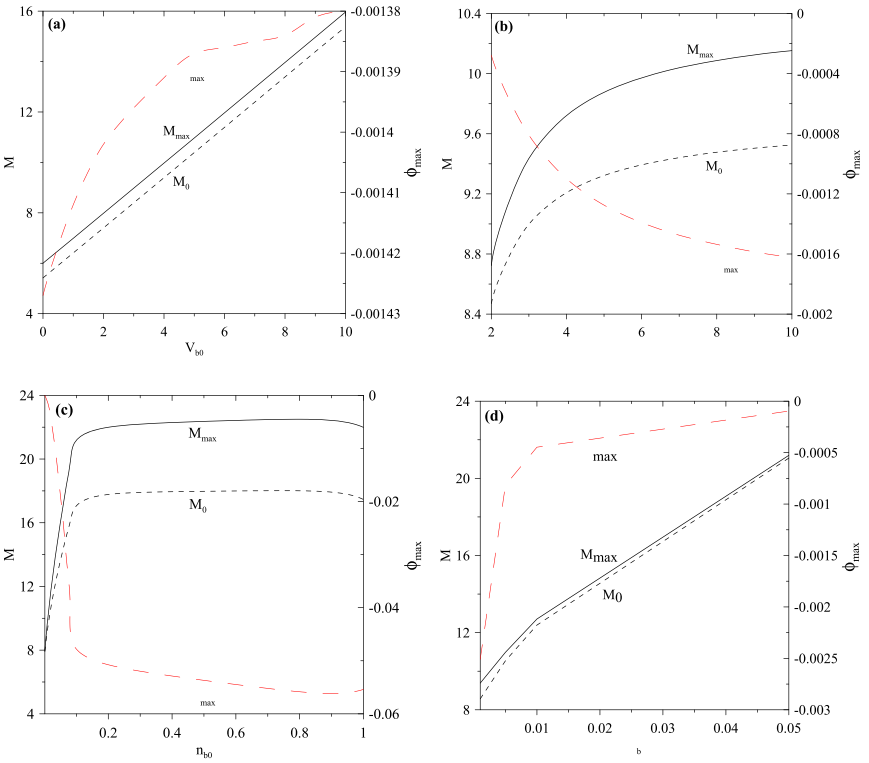

FIG. 6. Electron-acoustic solitons: variation of critical Mach number, M_0(dashed curves), maximum Mach number, M_{max} (solid curves), and maximum value of the potential, ϕ_{max} (long-dashed red curve) with (a) V_{b0}, (b) κ, (c) n_{b0}, and (d) σ_b for the parameters of Fig. 2. Here the Y-axis on the left hand side (LHS) and the right hand side (RHS) shows the scale for Mach number and maximum electric potential amplitude ϕ_{max}, respectively.

$M_{max} - M_0$, remains constant throughout. ϕ_{max} increases gradually with V_{b0} till $V_{b0} = 5$. Then, ϕ_{max} remains constant till $V_{b0} = 8$ followed again by an increase. Unlike slow and fast ion-acoustic solitons, electron-acoustic soliton does not support any transition from negative to positive potential soliton or the coexistence of both positive and negative potential solitons. Moreover, electron-acoustic soliton does not support any "forbidden gap" region unlike slow and fast ion-acoustic solitons. From panel (b), we observe that M_0, M_{max}, and $M_{max} - M_0$ increase gradually with κ. However, ϕ_{max} decreases gradually with the increase in κ. This trend shown by ϕ_{max} is contrary to the trend shown by slow and fast ion-acoustic solitons. ϕ_{max} increases gradually for both slow and fast ion-acoustic solitons. Further, the existence domain for electron-acoustic soliton is greater than both slow and fast ion-acoustic solitons. From panel (c), we observe that M_0, M_{max}, and $M_{max} - M_0$ increase gradually initially and then remain constant with n_{b0}, while ϕ_{max} decreases initially and then remains constant. It is observed from panel (d) that M_0 and M_{max} increase gradually with σ_b, while ϕ_{max} shows a sudden increase till $\sigma_b = 0.005$ and then increases gradually with further increase in σ_b.

The existence domain for the electron-acoustic solitons as a function of n_{i0} and σ_i was explored for the normalized parameters corresponding to Fig. 2. M_0, M_{max}, and $M_{max} - M_0$ were found to remain constant with n_{i0}. ϕ_{max} remains constant till $n_{i0} = 0.04$ followed by an increase till $n_{i0} = 0.05$. It is found that σ_i does not affect the evolution of electron-acoustic solitons (not shown).

IV. DISCUSSION AND CONCLUSIONS

Occurrence and existence domain of ESWs in a magnetized four-component plasma comprising of hot heavier ions (He^{++}), hot protons, electron beam, and suprathermal electrons have been examined for lunar wake plasma parameters. Three modes, viz., slow and fast ion-acoustic modes and electron-acoustic modes, exist.

The slow and fast ion-acoustic mode is found to support both positive and negative potential solitons as well as the coexistence of both polarity solitons. In addition, they support a "forbidden gap," the region in which the soliton solution ceases to propagate. The occurrence of the "forbidden gap" can be attributed to that the critical Mach number for the slow and fast ion-acoustic soliton becomes complex. Further, the slow ion-acoustic soliton is found to support both positive and negative polarity double layers. When $T_i = 4\ T_p$, the slow ion-acoustic mode ceases to exist and we only have fast ion-acoustic solitons. Over a narrow region of the electron beam velocity, V_{b0}, the fast ion-acoustic mode exhibits "anomalous behaviour." In such a region, the amplitude of the soliton decreases with the increase in the Mach number. As opposed to the slow ion-acoustic mode, fast ion-acoustic mode does not show any transition from positive potential soliton to negative potential soliton with respect to σ_i. Further, the amplitude of the slow ion-acoustic soliton is found to be lesser than that of the fast ion-acoustic soliton. Electron-acoustic soliton is found to support only negative potential solitons for parameters corresponding to the lunar wake plasma.

The maximum attainable amplitudes of the positive potential slow and fast ion-acoustic soliton are attributed to the requirement that the number density of heavier ions, n_i, and that of protons, n_p, should remain real, respectively. The limitation on the maximum attainable amplitude of negative potential slow and fast ion-acoustic soliton and electron-acoustic soliton is provided by the requirement that the number density of electron beam, n_b, should remain real, while,

for a limited range of parameters, the limitation on the negative potential slow ion-acoustic soliton is provided by the violation of the conditions $S(\phi, M) = 0$ at $\phi = \phi_{max}$ and $S(\phi, M) < 0$ for $0 < |\phi| < |\phi_{max}|$ to be satisfied by the Sagdeev pseudopotential for the soliton solution to exist. For slow-ion acoustic solitons, when double layer exists, the occurrence of double layer limits the maximum attainable amplitude of the soliton.

It is observed that the velocity of slow ion-acoustic mode is greater than the thermal velocity of heavier ions (V_{ti}), but is less than the thermal velocity of protons (V_{tp}). The velocity of fast ion-acoustic mode was found to be greater than the thermal velocity of protons (V_{tp}), but is less than the thermal velocity of beam electrons (V_{tb}). Further, it was found that the velocity of electron-acoustic mode is greater than the thermal velocity of beam electrons (V_{tb}) but is less than the thermal velocity of suprathermal electrons (V_{te}): $\sqrt{3}V_{ti} < V_{slow} < \sqrt{3}V_{tp} < V_{fast} < \sqrt{3}V_{tb} < V_{electron} < \sqrt{3}V_{te}$.

We apply our theoretical model to explain the observations of the electrostatic waves in the lunar wake during the first lunar wake flyby of the ARTEMIS mission.[14] Tao *et al.*[14] reported that the frequency range of the waves lies mostly between $0.1f_{pe}$ and $0.4f_{pe}$. However, in the middle of the flyby, the frequency occasionally reduces to $0.01f_{pe}$; f_{pe} is the electron plasma frequency ($f_{pe} = 3237.78$ Hz). Further, they reported that the electric field amplitude parallel to the ambient magnetic field roughly varies from 5 to 15 mV m^{-1}. The phase velocity of the wave was reported to be around few thousands of km s^{-1}, while the wavelength was found to vary from few hundreds to a couple of thousands of meters. For numerical estimation of the physical properties of the electrostatic waves, we have used the parameters:[14,15] temperature of electron, $T_e = 28$ eV, and total number density of electrons, $n_0 = 0.13$ cm^{-3}. For these parameters, the ion-acoustic speed $C_a = 52$ km s^{-1}, the effective hot electron Debye length $\lambda_{de} = 109$ m, and the effective proton plasma frequency, $f_{pp} = 474.69$ Hz.

As an illustration of the frequencies generated by these three types of solitons, a typical fast Fourier transform (FFT) power spectra of the electric fields corresponding to the normalized parameters $n_{i0} = 0.05$, $n_{b0} = 0.01$, $\sigma_p = 0.2$, $\sigma_i = 0.4$, $\sigma_b = 0.0025$, $V_{b0} = 10$, and $\kappa = 6$ are shown in Fig. 7. Corresponding to the normalized parameter, the fast ion-acoustic mode supports the coexistence of both positive and negative potential soliton. The blue curve depicts the FFT power spectra of the slow ion-acoustic soliton corresponding to $M = 0.56$. The frequency peak in the FFT power spectra occurs at 19.45 Hz, corresponding to $\sim 0.006 f_{pe}$. The frequency, f, in the range of $\sim$(6.49–84.33) Hz, corresponding to $\sim(0.002–0.03)f_{pe}$, contributes maximum to the electric field structure. The red and yellow curves depict the FFT power spectra of the positive and negative potential fast ion-acoustic solitons, respectively, corresponding to $M = 1.30$. The frequency peak in the spectra for the positive soliton occurs at 37.67 Hz, corresponding to $\sim 0.01 f_{pe}$, while for the negative soliton it occurs at 15.07 Hz, corresponding to $\sim 0.005 f_{pe}$. The frequency, f, in the range of $\sim$(7.53–1091.44) Hz, corresponding to $\sim(0.002–0.3)f_{pe}$, contributes maximum to the electric field structure of the positive potential soliton. The frequency, f, in the range of $\sim$(7.53–2409.9) Hz, corresponding to $\sim(0.002–0.74)f_{pe}$, contributes maximum to the electric field structure of the negative potential soliton. The FFT power spectra of the electron-acoustic soliton for $M = 15.85$ is depicted by a green curve. Here, the peak in the spectra occurs at 550.81 Hz, corresponding to $\sim 0.17 f_{pe}$. The frequency, f, in the range of $\sim$(183.65– 6251.73) Hz, corresponding to $\sim(0.06–1.9)f_{pe}$ contributes maximum to the electric field structure. The upper limit on the frequency, f, is taken at the cutoff power of -70 dB for slow ion-acoustic and positive potential fast ion-acoustic soliton and electron-acoustic soliton, while for the negative potential fast ion-acoustic soliton, the cutoff power is considered as -35 dB. The cutoff power is taken at a value beyond which the power spectrum approaches noise levels.

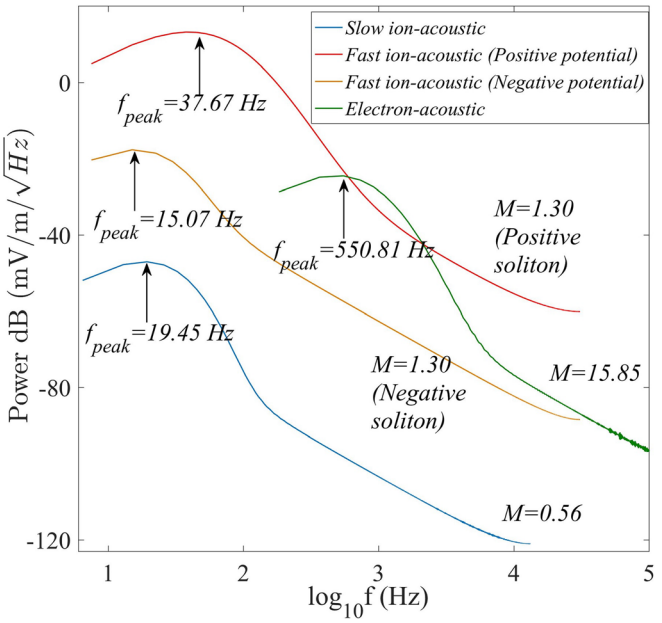

FIG. 7. The fast Fourier transform (FFT) power spectra of the electric field corresponding to the parameters of Fig. 1 and $V_{b0} = 10$. Here, $M = 0.56$ and $M = 1.3$ for slow (blue curve) and fast (red and yellow curves) ion-acoustic solitons, respectively, and $M = 15.85$ (electron-acoustic soliton, green curve).

We have shown that solitons exists between the Mach number range, $(M_0 \leq M \leq M_{max})$ for a given V_{b0}. Hence, corresponding to each of the three soliton types, we have a range of electric field amplitudes, widths, soliton velocities, and peak frequencies corresponding to the maximum power in the spectrum. For $V_{b0} = 10$, the velocity of the slow ion-acoustic soliton varies as $\sim$(28.94–29.11) km s^{-1}. The electric field amplitude lies in the range $\sim$(0.0005–0.03) mV m^{-1}. The width lies in the range $\sim$(1215.14–257.43) m. Here, the width corresponds to the full width at half maximum and the higher values of the width correspond to the lower soliton velocity. The peak frequency varies in the range $\sim$(6.48–39.08) Hz, corresponding to $\sim(0.002–0.01)f_{pe}$. The velocity, electric field, width, and peak frequency for the positive potential fast ion-acoustic soliton varies, respectively, in the range $\sim$(66.01–71.65) km s^{-1}, $\sim$(5.73–20.03) mV m^{-1}, $\sim$(674.11–253.06) m, and $\sim$(29.58–64.12) Hz corresponding to

$\sim(0.009–0.02)f_{pe}$, while for the negative potential fast ion-acoustic soliton, the velocity, electric field, width, and peak frequency vary, respectively, as $\sim(66.06–70.51)\,\mathrm{km\,s^{-1}}$, $\sim(0.001–0.34)\,\mathrm{mV\,m^{-1}}$, $\sim(7548.27–645.75)\,\mathrm{m}$, and $\sim(3.69–31.55)$ Hz corresponding to $\sim(0.001–0.01)f_{pe}$. For the electron-acoustic soliton, the velocity, electric field, width, and peak frequency varies, respectively, in the range $\sim(799.33–826.40)\,\mathrm{km\,s^{-1}}$, $\sim(0.003–0.1)\,\mathrm{mV\,m^{-1}}$, $\sim(1588.19–438.49)\,\mathrm{m}$, and $\sim(179.06–554.62)\,\mathrm{Hz}$ corresponding to $\sim(0.06–0.2)f_{pe}$.

As all three modes exists simultaneously in the lunar wake,[15] taken together, the velocities varying as $\sim$28–826 km s^{-1} matches with the observed phase velocities varying as a few thousands of km s^{-1}. The electric field amplitude in the range $\sim(0.0005–20)$ mV m^{-1} matches with the observed range of (5–15) mV m^{-1}. The width varying as few hundreds of meters to a couple of thousands of meters agrees with the observed wavelength. The frequency of the solitons varying as $\sim(0.001–0.2)f_{pe}$ can explain the observed low frequency waves around $0.01f_{pe}$ as well as the high frequency waves around $(0.1–0.4)f_{pe}$. Hence, all three modes taken together can provide a good explanation for the observed electrostatic waves in the lunar wake.

ACKNOWLEDGMENTS

G.S.L. thanks the National Academy of Sciences, India, for the support under the NASI-Senior Scientist Platinum Jubilee Fellowship scheme.

[1]R. E. Ergun, C. W. Carlson, J. P. McFadden, F. S. Mozer, L. Muschietti, I. Roth, and R. J. Strangeway, Phys. Rev. Lett. **81**, 826 (1998).
[2]S. R. Bounds, R. F. Pfaff, S. F. Knowlton, F. S. Mozer, M. A. Temerin, and C. A. Kletzing, J. Geophys. Res. **104**, 28709, https://doi.org/10.1029/1999JA900284 (1999).
[3]H. Kojima, H. Matsumoto, S. Chikuba, S. Horiyama, M. Ashour-Abdalla, and R. R. Anderson, J. Geophys. Res. **102**, 14439, https://doi.org/10.1029/97JA00684 (1997).
[4]H. Matsumoto, H. Kojima, T. Miyatake, Y. Omura, M. Okada, I. Nagano, and M. Tsutsui, Geophys. Res. Lett. **21**, 2915, https://doi.org/10.1029/94GL01284 (1994).
[5]H. Matsumoto, X. H. Deng, H. Kojima, and R. R. Anderson, Geophys. Res. Lett. **30**, 1326, https://doi.org/10.1029/2002GL016319 (2003).
[6]S. D. Bale, P. J. Kellogg, D. E. Larson, R. P. Lin, K. Goetz, and R. P. Lepping, Geophys. Res. Lett. **25**, 2929, https://doi.org/10.1029/98GL02111 (1998).
[7]F. S. Mozer, O. V. Agapitov, A. Artemyev, J. F. Drake, V. Krasnoselskikh, S. Lejosne, and I. Vasko, Geophys. Res. Lett. **42**, 6273, https://doi.org/10.1002/2015GL063946 (2015).
[8]I. Y. Vasko, O. V. Agapitov, F. S. Mozer, J. Bonnell, A. V. Artemyev, V. V. Krasnoselskikh, G. Reeves, and G. Hospodarsky, Geophys. Res. Lett. **44**, 4575, https://doi.org/10.1002/2017GL074026 (2017).
[9]A. Mangeney, C. Salem, C. Lacombe, J. L. Bougeret, C. Perche, R. Manning, P. J. Kellogg, K. Geotz, S. J. Monson, and J. M. Bosqued, Ann. Geophys. **17**, 307 (1999).
[10]D. M. Malaspina, D. L. Newman, L. B. Willson, K. Goetz, P. J. Kellogg, and K. Kerstin, J. Geophys. Res.—Space Phys. **118**, 591 (2013).
[11]K. Hashimoto, M. Hashitani, Y. Kasahara, Y. Omura, M. N. Nishino, Y. Saito, S. Yokota, T. Ono, H. Tsunakawa, H. Shibuya, M. Matsushima, H. Shimizu, and F. Takahashi, Geophys. Res. Lett. **37**, L19204, https://doi.org/10.1029/2010GL044529 (2010).
[12]K. W. Ogilvie, J. T. Steinberg, R. J. Fitzenreiter, C. J. Owen, A. J. Lazarus, W. M. Farrell, and R. B. Torbert, Geophys. Res. Lett. **23**, 1,255, https://doi.org/10.1029/96GL01069 (1996).
[13]S. Wiehle, F. Plaschke, U. Motschmann, K. H. Glassmeier, H. U. Auster, V. Angelopoulos, J. Mueller, H. Kriegel, E. Georgescu, J. Halekas, D. G. Sibeck, and J. P. McFadden, Planet. Space Sci. **59**, 661 (2011).
[14]J. B. Tao, R. E. Ergun, D. L. Newman, J. S. Halekas, L. Andersson, V. Angelopoulos, J. W. Bonnell, J. P. McFadden, C. M. Cully, H. U. Auster, K. H. Glassmeier, D. Larson, W. Baumjohann, and M. V. Goldman, J. Geophys. Res. **117**, A03106, https://doi.org/10.1029/2011JA017364 (2012).
[15]R. Rubia, S. V. Singh, and G. S. Lakhina, J. Geophys. Res. Space Phys. **122**, 9134–9147 (2017).
[16]R. Z. Sagdeev, "Cooperative phenomena and shock waves in collisionless plasmas," in *Reviews of Plasma Physics 4*, edited by M. A. Leontovich (Consultants Bureau, New York, 1966), p. 23.
[17]H. Washimi and T. Taniuti, Phys. Rev. Lett. **17**, 996 (1966).
[18]K. Watanabe and T. Taniuti, J. Phys. Soc. Jpn. **43**, 1819 (1977).
[19]G. C. Das and S. G. Tagare, Plasma Phys. **17**, 1025 (1975).
[20]M. Q. Tran, Phys. Scr. **20**, 317 (1979).
[21]B. Buti, Phys. Lett. A **76**, 251 (1980).
[22]S. S. Dash and B. Buti, Phys. Lett. **81A**, 347 (1981).
[23]S. P. Gary and R. L. Tokar, Phys. Fluids **28**, 2439 (1985).
[24]G. Chanteur and M. Raadu, Phys. Fluids **30**, 2708 (1987).
[25]N. Dubouloz, R. Pottelette, M. Malingre, and R. A. Treumann, Geophys. Res. Lett. **18**, 155, https://doi.org/10.1029/90GL02677 (1991).
[26]S. S. Ghosh and A. N. S. Iyengar, Phys. Plasmas. **4**, 2139 (1997).
[27]S. V. Singh and G. S. Lakhina, Planet. Space Sci. **49**, 107 (2001).
[28]F. Verheest, T. Cattaert, and M. A. Hellberg, Space Sci. Rev. **121**, 299 (2005).
[29]T. Cattaert, F. Verheest, and M. A. Hellberg, Phys. Plasmas. **12**, 042901 (2005).
[30]A. P. Kakad, S. V. Singh, R. V. Reddy, G. S. Lakhina, S. G. Tagare, and F. Verheest, Phys. Plasmas **14**, 052305 (2007).
[31]G. S. Lakhina, A. P. Kakad, S. V. Singh, and F. Verheest, Phys. Plasmas **15**, 062903 (2008).
[32]G. S. Lakhina, S. V. Singh, A. P. Kakad, F. Verheest, and R. Bharuthram, Nonlinear Processes Geophys. **15**, 903 (2008).
[33]G. S. Lakhina, S. V. Singh, A. P. Kakad, M. L. Goldstein, A. F. Vinas, and J. S. Pickett, J. Geophys. Res. **114**, A09212, https://doi.org/10.1029/2009JA014306 (2009).
[34]N. S. Saini, I. Kourakis, and M. A. Hellberg, Phys. Plasmas **16**, 062903 (2009).
[35]S. Sultana, I. Kourakis, N. S. Saini, and M. A. Hellberg, Phys. Plasmas **17**, 032310 (2010).
[36]T. K. Baluku, M. A. Hellberg, and F. Verheest, EPL **91**, 15001 (2010).
[37]N. S. Saini and I. Kourakis, Plasma Phys. Controlled Fusion **52**, 075009 (2010).
[38]M. Tribeche and L. Djebarni, Phys. Plasmas **17**, 124502 (2010).
[39]S. Devanandhan, S. V. Singh, and G. S. Lakhina, Phys. Scr. **84**, 025507 (2011).
[40]S. V. Singh, G. S. Lakhina, R. Bharuthram, and S. R. Pillay, Phys. Plasmas. **18**, 122306 (2011).
[41]S. Devanandhan, S. V. Singh, G. S. Lakhina, and R. Bharuthram, Nonlinear Processes Geophys. **18**, 627634 (2011).
[42]S. Devanandhan, S. V. Singh, G. S. Lakhina, and R. Bharuthram, Phys. Plasmas. **19**, 082314 (2012).
[43]O. R. Rufai, R. Bharuthram, S. V. Singh, and G. S. Lakhina, Phys. Plasmas **19**, 122308 (2012).
[44]S. K. Maharaj, R. Bharuthram, S. V. Singh, and G. S. Lakhina, Phys. Plasmas **19**, 072320 (2012).
[45]S. K. Maharaj, R. Bharuthram, S. V. Singh, and G. S. Lakhina, Phys. Plasmas **19**, 122301 (2012).
[46]S. V. Singh, S. Devanandhan, G. S. Lakhina, and R. Bharuthram, Phys. Plasmas **20**, 012306 (2013).
[47]E. Saberian, A. Esfandyari-Kalejahi, A. Rastkar-Ebrahimzadeh, and M. Afsari-Ghazi, Phys. Plasmas. **20**, 032307 (2013).
[48]F. Nsengiyumva, M. A. Hellberg, F. Verheest, and R. L. Mace, Phys. Plasmas **21**, 102301 (2014).
[49]S. S. Ghosh and A. N. S. Iyengar, Phys. Plasmas. **21**, 082104 (2014).
[50]G. S. Lakhina, S. V. Singh, and A. P. Kakad, Phys. Plasmas **21**, 062311 (2014).
[51]C. P. Olivier, S. K. Maharaj, and R. Bharuthram, Phys. Plasmas **22**, 082312 (2015).
[52]S. K. Maharaj, R. Bharuthram, S. V. Singh, and G. S. Lakhina, Phys. Plasmas **22**, 032313 (2015).
[53]G. S. Lakhina and S. V. Singh, Sol. Phys. **290**, 3033 (2015).
[54]R. Rubia, S. V. Singh, and G. S. Lakhina, Phys. Plasmas **23**, 062902 (2016).

[55]I. B. Bernstein, J. M. Greene, and M. D. Kruskal, Phys. Rev. **108**, 546 (1957).
[56]H. Schamel, Phys. Scr. **T2/1**, 228 (1982).
[57]H. Schamel, Phys. Plasmas **7**, 4831 (2000).
[58]H. Schamel, Phys. Plasmas **22**, 042301 (2015).
[59]Y. Omura, H. Matsumoto, T. Miyake, and H. Kojima, J. Geophys. Res. **101**, 2685, https://doi.org/10.1029/95JA03145 (1996).
[60]M. V. Goldman, M. M. Oppenheim, and D. L. Newman, Geophys. Res. Lett. **26**, 1821, https://doi.org/10.1029/1999GL900435 (1999).
[61]M. Oppenheim, D. L. Newman, and M. V. Goldman, Phys. Rev. Lett. **83**(2), 2344 (1999).
[62]N. Singh and G. Khazanov, J. Geophys. Res. **108**, 8007, https://doi.org/10.1029/2002JA009436 (2003).
[63]J. Dombeck, C. Cattell, J. Crumley, W. K. Peterson, H. L. Collin, and C. Kletzing, J. Geophys. Res. **106**, 19013, https://doi.org/10.1029/2000JA000355 (2001).
[64]S. S. Ghosh and G. S. Lakhina, Nonlinear Processes Geophys. **11**, 219 (2004).